

Calibration of luminosity correlations of gamma-ray bursts using quasars

Sarveshkumar Purohit* and Shantanu Desai†

*Department of Artificial Intelligence, Indian Institute of Technology, Hyderabad, Telangana-502284, India and
Department of Physics, Indian Institute of Technology, Hyderabad, Telangana-502284, India*

In order to test the efficacy of Gamma-ray Bursts (GRBs) as cosmological probes, we characterize the scatter in the correlations between six pairs of GRB related observables, which have previously also been studied in [1]. However, some of these observables depend on the luminosity distance, for which one needs to assume an underlying cosmological model. In order to circumvent this circularity problem, we use X-ray and UV fluxes of quasars as distance anchors to calculate the luminosity distance in a model-independent manner, which in turn gets used to calculate the GRB-related quantities. We find that all the six pairs of regression relations show a high intrinsic scatter for both the low and high redshift sample. This implies that these GRB observables cannot be used as model-independent cosmological probes.

I. INTRODUCTION

Gamma-ray bursts (GRBs) are single-shot explosions located at cosmological distances, which were first detected in 1960s and have been observed over ten decades in energies from keV to over 10 TeV range [2, 3]. They are located at cosmological distances, although a distinct time-dilation signature in the light curves is yet to be demonstrated [4]. Because of their high energies and cosmological distances, they also have proved to be very good probes of fundamental physics, such as testing of Lorentz invariance violation and quantum gravity [5]. GRBs are traditionally divided into two categories based on their durations, with long (short) GRBs lasting more (less) than two seconds [6]. Long GRBs are usually associated with core-collapse supernovae [7] and short GRBs with neutron star mergers [8]. There are however many exceptions to this conventional dichotomy, and many claims for additional GRB sub-classes have also been discussed in literature [9, 10] (and references therein).

GRBs have also been proposed as distance indicators or standard candles over the past two decades due to a large number of observed correlations between various GRB observables in both the prompt and afterglow emission phase [11–16]. These correlations have often been used to estimate cosmological parameters [17]. However, there is an inherent circularity problem in using the GRB observables as cosmological probes, since the calculation of some of these observables is based on an underlying cosmological model. To get around this circularity problem, two methodologies have been used in literature. One way is to simultaneously constrain the GRB correlations along with the cosmological parameters [18]. Alternately, a large number of ancillary probes have also been used to obtain cosmology-independent estimates of distances corresponding to the GRB redshift such as Type Ia SN, cosmic chronometers, BAO $H(z)$ measurements, X-ray and UV luminosities of quasars, galaxy clusters etc [19] (and references therein).

Here, we focus on correlations between six pairs of GRB observables: $\tau_{lag} - L$, $V - L$, $E_{peak} - L$, $E_{peak} - E_{\gamma}$, $\tau_{RT} - L$, $E_{peak} - E_{iso}$, which were first proposed in [20]. We note that among the above correlations, the $E_{peak} - E_{\gamma}$ relation is often referred to as the Amati relation in literature [21]. The aforementioned work simultaneously fitted for cosmology and as well any possible correlations [20]. These same correlations were then analyzed by obtaining model-independent distances to GRBs using the Pantheon compilation [22] of Type Ia SN in [1] (T21, hereafter). Here, we carry out a variant of the analysis done in [1], by using X-ray and UV luminosities of quasars instead of Type Ia SN to probe the same correlations first considered in [20]. We note that quasars have previously been used to probe the efficacy of the Amati relation in GRBs [23] using the datasets in [18, 24, 25].

The outline of this manuscript is as follows. We discuss the datasets used in this work in Sect. II. Our analysis and results can be found in Sect. III. We conclude in Sect. IV.

II. DATASETS

We use the same GRB datasets as those considered in [20]. This work considered a sample of 116 long GRBs with redshifts between 0.17 to 8.2. This sample consisted of GRBs observed by SWIFT until 2012 in conjunction with

*sarveshpurohit84@gmail.com

†shntn05@gmail.com

additional GRBs from the pre-SWIFT era [26]. The observables assembled for each GRB consists of bolometric peak flux (P_{bolo}), bolometric fluence (S_{bolo}), beaming factor (F_{beam}), time lag between low and high energy photon light curves (τ_{lag}), peak energy of the spectrum (E_{peak}), minimum rise time of the peaks for which the light curve rise by half its peak flux (τ_{RT}), and the variability of the light curve (V). More details can also be found in [20]. In addition to the values, the 1σ error bars were also provided for each of the above observables in [20]. Among these variables, τ_{RT} , E_{peak} , τ_{lag} , and V were obtained directly from the light curves, whereas P_{bolo} and S_{bolo} can be obtained from the observed GRB spectrum as outlined in [20]. In order to test for potential correlations, additional quantities such as the isotropic peak luminosity (L), isotropic equivalent energy (E_{iso}), collimation-corrected energy (E_{γ}) depend on the luminosity distance (d_L), which in turn need an underlying cosmological model. We now discuss the quantities which depend on d_L . The relation between L and P_{bolo} is given by:

$$L = 4\pi d_L^2 P_{bolo}, \quad (1)$$

E_{iso} is related to D_L using:

$$E_{iso} = 4\pi d_L^2 S_{bolo} (1+z)^{-1} \quad (2)$$

Finally E_{γ} is given by:

$$E_{\gamma} = 4\pi d_L^2 S_{bolo} F_{beam}, \quad (3)$$

where F_{beam} is the beaming factor which was estimated using the empirical formula derived in [27].

This dataset was used to study six different pairs of luminosity correlations: $\tau_{lag} - L$, $V - L$, $E_{peak} - L$, $E_{peak} - E_{\gamma}$, $\tau_{RT} - L$, $E_{peak} - E_{iso}$, where some of the above variables were scaled according to redshift as explained in the next section. To circumvent this circularity problem in calculating some of the above variables in a model agnostic manner, a simultaneous fit to a linear regression between the above variables and the underlying cosmology model was simultaneously done [20]. The intrinsic scatter of the $V - L$ correlation was found to be very large, but the other variables had a tight correlation with a negligible redshift evolution. These same set of correlations between the variables were then re-examined using a theory-agnostic approach without assuming an underlying cosmological model [1]. For this purpose, a model-independent estimate of d_L at each GRB redshift was obtained using deep learning and Gaussian process based regression using Type Ia supernova data. This work also tested for a redshift evolution for the same six regression relations (considered in [20]) by dividing the GRB dataset into a low redshift and high redshift sample. Among these, only $E_p - E_{\gamma}$ was found to contain no redshift evolution [1].

A. Quasar dataset

In order to obtain the distance corresponding to a given GRB redshift, instead of Type Ia SN, we use quasars as distance anchors. Quasars contain Active galactic nuclei, where the energy release occurs due to the accretion onto a supermassive black hole. Quasars have been detected up to a redshift of $z = 7$ and are therefore comparable to those found for GRBs. Quasars have been observed throughout the electromagnetic spectrum [28]. A tight scaling relation between the optical-UV flux at rest frame wavelength of 2500 Å and X-ray flux at rest frame energy of 2 keV of a quasar has been asserted (with a scatter of around 0.12 dex), which is independent of redshift [29].

The luminosity distance (D_L) at a given redshift is obtained from the quasar X-ray and UV flux as follows [29, 30]:

$$\log D_L = \frac{[\log F_X - \beta - \gamma(\log F_{UV} + 27.5)]}{2(\gamma - 1)} - 0.5 \log(4\pi) + 28.5, \quad (4)$$

where F_X and F_{UV} are the flux densities (in $\text{erg/s/cm}^2/\text{Hz}$) $\beta \approx 8.2$ and $\gamma = 0.6$. This relation was obtained assuming a Hubble constant value of $H_0 = 70 \text{ km/sec/Mpc}$. Lusso et al [30] constructed a clean sample of 2,421 optically selected quasars spanning the redshift range $0.006 \leq z \leq 7.52$ where distance modulus (DM) and associated errors were obtained using D_L from the above equation as below:

$$\text{DM} = 5 \log(D_L) - 5 \log(10\text{pc}) \quad (5)$$

Therefore one can obtain the distance modulus for each quasar redshift from the quasar X-ray and UV fluxes.

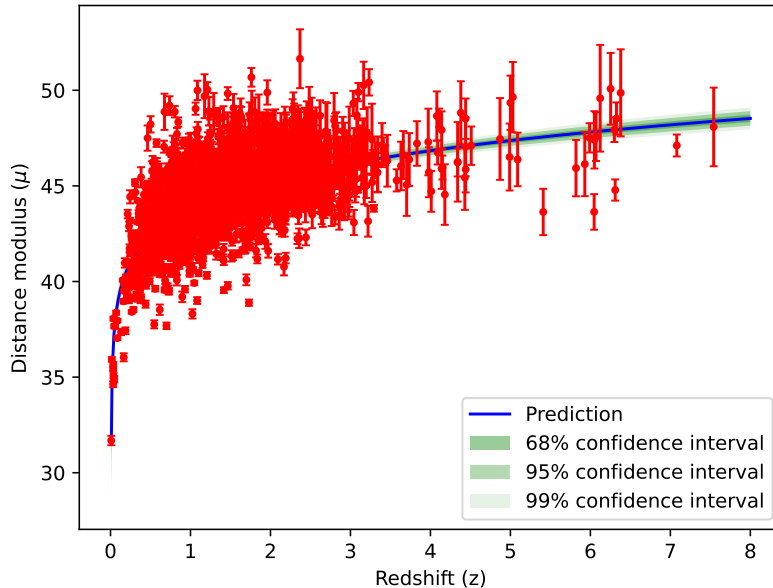


FIG. 1: Reconstruction of the distance modulus of μ with GPR using X-ray and UV fluxes for 2,421 quasars.

III. ANALYSIS AND RESULTS

The first step in the analysis involves obtaining a model-independent estimate of D_L from the quasar Dataset. As mentioned in the previous section, we start with the distance modulus (μ) and redshift (z) data for 2,421 quasars. With this data, we carry out a non-parametric reconstruction of distance modulus (μ) at any redshift z using Gaussian Process Regression (GPR). GPR is a generalization of a Gaussian distribution, characterized by a mean and a covariance function (usually called the kernel function) [31]. More details about GPR can be found in our previous works [19, 32–39]. For the GPR implementation, we use the publicly available Python package `sklearn` [40] to reconstruct the distance modulus (μ) as a function of redshift (z) as follows:

$$k(x, x') = \text{ConstantKernel}() + 1.0 * \text{DotProduct}(1) ** 0.1 \quad (6)$$

The kernel we have used is a sum of linear and constant kernels. A linear kernel with an exponent captures relations in the data, and a constant kernel is used to scale magnitude. The GPR reconstruction of distance modulus (μ) and the associated 1σ error bars can be found in Fig. 1. Once we have reconstructed distance modulus (μ) at any z , we can estimate the luminosity distance (D_L) from μ , by inverting Eq. 5. The errors in D_L can be obtained using standard error propagation. Once we obtain D_L for every GRB redshift, we can calculate L and E_{iso} and using Eq. 1 and Eq. 2, respectively.

We then construct the following linear regression relations between the six aforementioned GRB quantities in log

space as follows:

$$\log \frac{L}{\text{erg s}^{-1}} = a_1 + b_1 \log \frac{\tau_{\text{lag},i}}{0.1\text{s}}, \quad (7)$$

$$\log \frac{L}{\text{erg s}^{-1}} = a_2 + b_2 \log \frac{V_i}{0.02}, \quad (8)$$

$$\log \frac{L}{\text{erg s}^{-1}} = a_3 + b_3 \log \frac{E_{p,i}}{300\text{keV}} \quad (9)$$

$$\log \frac{E_\gamma}{\text{erg}} = a_4 + b_4 \log \frac{E_{p,i}}{300\text{keV}}, \quad (10)$$

$$\log \frac{L}{\text{erg s}} = a_5 + b_5 \log \frac{\tau_{\text{RT},i}}{0.1\text{s}}, \quad (11)$$

$$\log \frac{E_{\text{iso}}}{\text{erg}} = a_6 + b_6 \log \frac{E_{p,i}}{300\text{keV}} \quad (12)$$

where $\tau_{\text{RT},i} = \tau_{\text{RT}}/(1+z)$, $\tau_{\text{lag},i} = \tau_{\text{lag}}/(1+z)$, $V_i = V(1+z)$ and $E_{p,i} = E(1+z)$.

To get the best-fit parameters for each of the above equations, we apply the D'Agostini's likelihood which incorporates errors in both the ordinate and abscissa [41]:

$$\mathcal{L}(\sigma_{\text{int}}, a, b) \propto \prod_i \frac{1}{\sqrt{\sigma_{\text{int}}^2 + \sigma_{y_i}^2 + b^2 \sigma_{x_i}^2}} \times \exp \left[-\frac{(y_i - a - bx_i)^2}{2(\sigma_{\text{int}}^2 + \sigma_{y_i}^2 + b^2 \sigma_{x_i}^2)} \right], \quad (13)$$

where x and y denote the abscissa and ordinate and σ_{x_i} and σ_{y_i} are the corresponding errors; σ_{int} denotes the intrinsic scatter in each regression relation. To get the best-fit values of each of the parameters, we do Bayesian regression and sample the posterior using the `emcee` MCMC sampler [42].

In order to test if the aforementioned correlations vary with redshift, similar to [1], we bifurcate the GRB dataset into two subsamples corresponding to the following redshift bins: the low- z sample ($z \leq 1.4$) which consists of 50 GRBs, and the high- z sample ($z > 1.4$) which consists of 66 GRBs. We investigate the redshift dependence of luminosity correlations for these two subsamples. We also show the results for the full GRB sample.

The best-fit intervals at 68%, 90%, and 99% credible intervals for all six regression relations can be found in Fig. 2 for the full GRB sample as well as after bifurcating the sample based on redshift. The scatter plots between the six pairs of variables along with the best-fits are shown in Fig. 3. We find that our results for the slope, intercept and intrinsic scatter for almost all the six scaling relations are consistent with that obtained in T21. The only exception is the $E_p - E_\gamma$ or Amati correlation, where we see an intrinsic scatter of 26-40%, whereas the intrinsic scatter was found to be $< 23\%$ in T21. We find that the values for the slope and intercept are consistent or at most $1 - 2\sigma$ discrepant between the low redshift and high redshift samples indicating negligible evolution of the scaling relations. Furthermore, all the six regression relations show a high intrinsic scatter of greater than 30%. This includes the Amati relation, where we get a large scatter of 47%, when we consider the full data sample, similar to our results of using galaxy clusters as distance anchors [19]. Therefore, the regression relations between these observables cannot be used as model-independent probes of cosmological parameters.

IV. CONCLUSIONS

In a recent work, T21 tested the empirical correlations among six pairs of GRB observables for 116 long GRBs (first considered in [20]) in order to test their efficacy as a cosmological probe. However, one needs an estimate of the luminosity distance, which depends on an underlying cosmological model to calculate some of these GRB observables. In order to get around this circularity problem, luminosity distances from Type Ia supernovae were used as distance anchors, and the corresponding distance at a given GRB redshift was obtained using ANN based regression.

In this work, we carry out the same exercise as T21, but use X-ray and UV fluxes of quasars instead of Type Ia supernovae in order to get the luminosity distance at a given GRB redshift. The interpolation has been done using Gaussian process regression. Similar to [1], we test the correlations for both the low redshift and high redshift sample, after bifurcating the dataset at $z = 1.4$. Our results for the best-fit values for all the six regression relations can be found in Table I. The marginalized credible intervals are shown in Fig. 2, whereas the scatter plots for the six regression relations are shown in Fig. 3. Our conclusions are as follows:

- Our slopes and intercepts agree with the corresponding results with T21 for both the low and high redshift as well as the full sample.

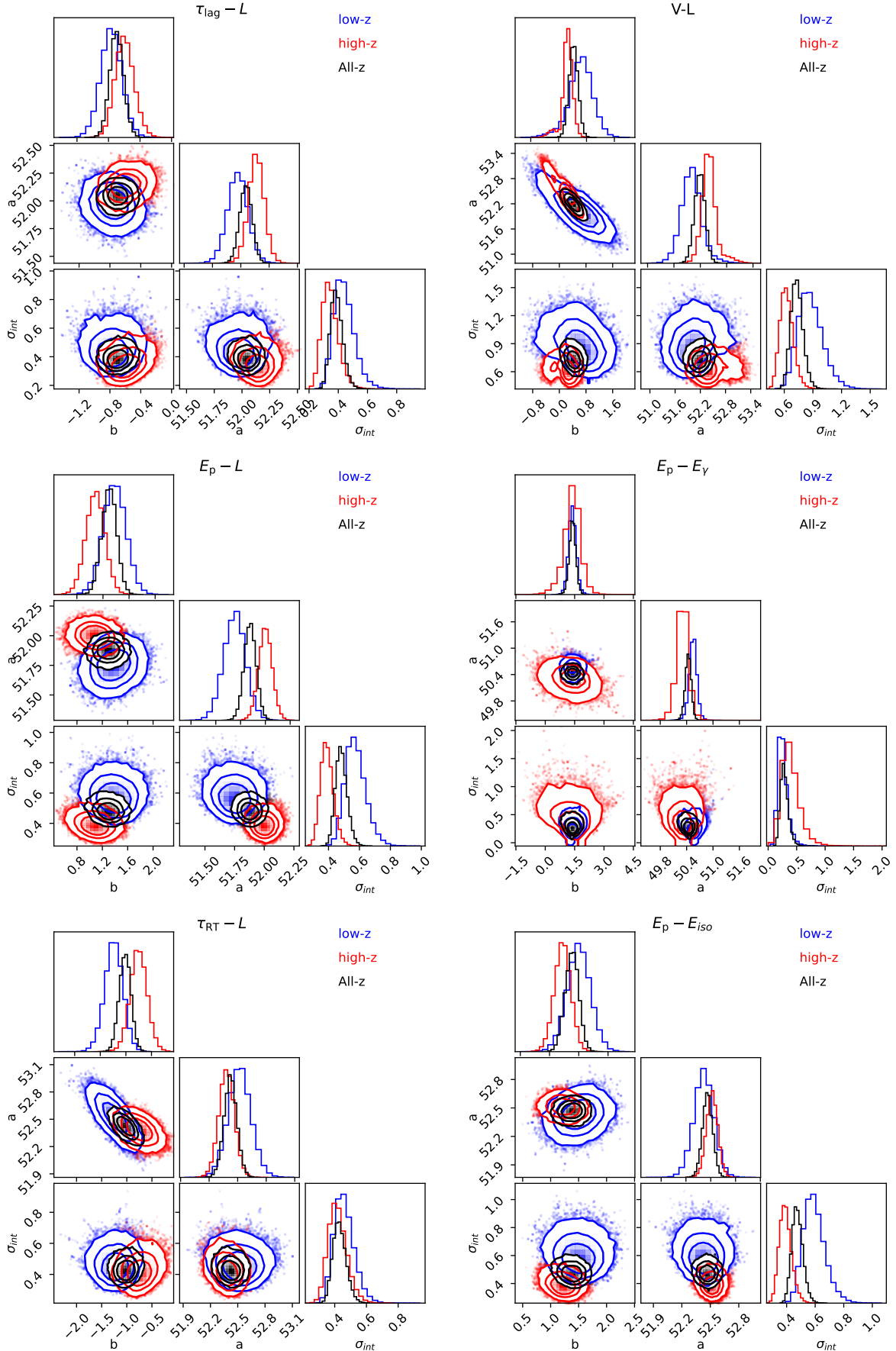


FIG. 2: The 68%, 90%, and 99% credible intervals along with the marginalized PDFs for the parameters for the regression relations between six pairs of GRB observables for low redshift ($z < 1.4$), high redshift ($z > 1.4$) as well as the full GRB dataset.

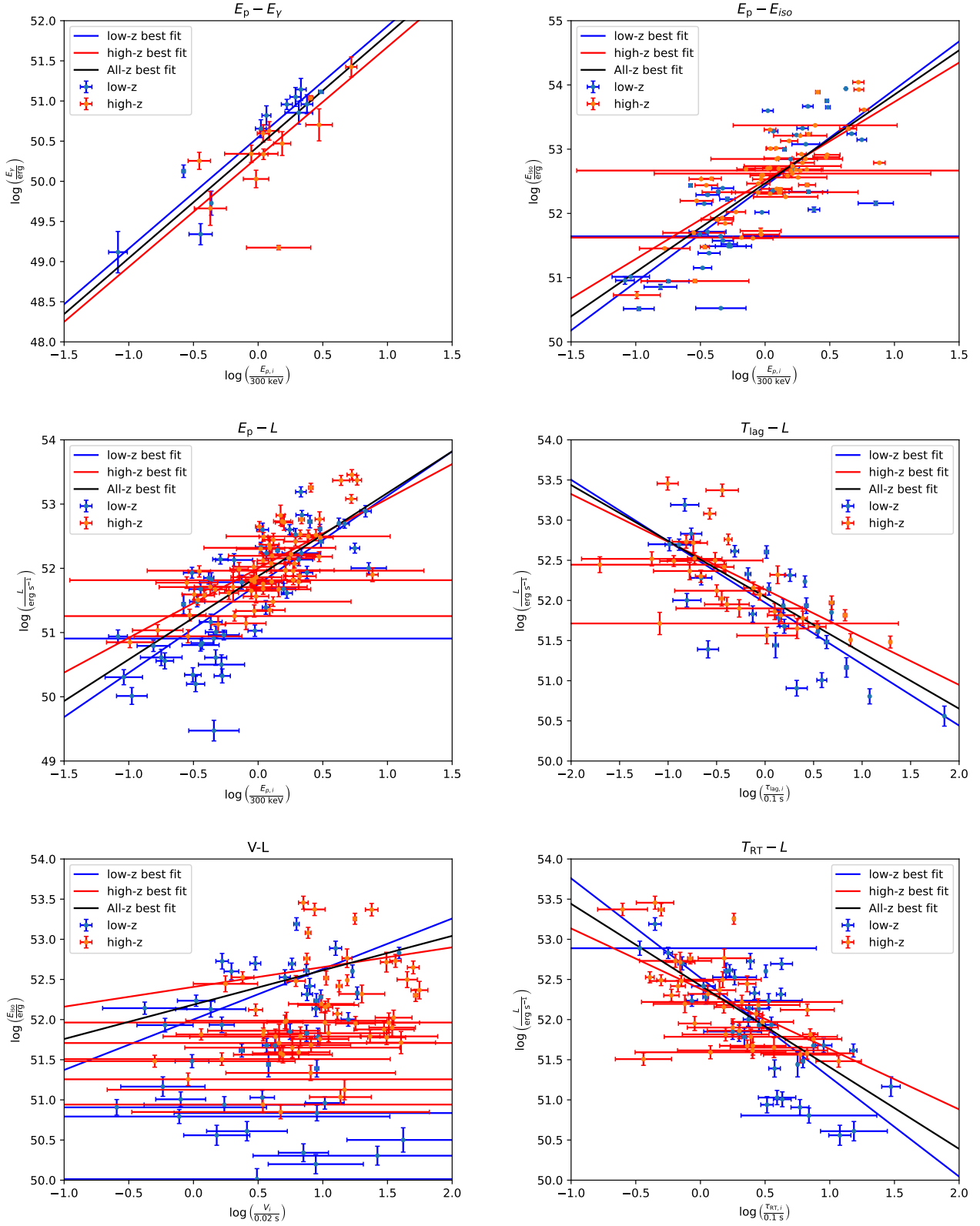


FIG. 3: The luminosity correlations for low- z (blue dots) and high- z (red dots) GRBs. Error bars denote the 1σ uncertainties. The lines depict the best-fit results, blue line for low- z GRBs, red line for high- z GRBs and black line for all- z GRBs.

TABLE I: The best-fitting parameters of GRB luminosity correlations. N is the number of GRBs in each subsample.

Correlation	Sample	N	a	b	σ_{int}
$\tau_{\text{ag}} - L$	low-z	37	51.97 ± 0.09	-0.77 ± 0.14	0.44 ± 0.07
	high-z	32	52.14 ± 0.07	-0.59 ± 0.12	0.35 ± 0.06
	All-z	69	52.04 ± 0.06	-0.69 ± 0.09	0.39 ± 0.04
$V - L$	low-z	47	52.00 ± 0.24	0.63 ± 0.36	0.88 ± 0.13
	high-z	57	52.41 ± 0.18	0.25 ± 0.17	0.63 ± 0.07
	All-z	104	52.19 ± 0.12	0.43 ± 0.13	0.73 ± 0.06
$E_p - L$	low-z	50	51.75 ± 0.09	1.38 ± 0.18	0.58 ± 0.07
	high-z	66	51.99 ± 0.06	1.08 ± 0.15	0.39 ± 0.04
	All-z	116	51.88 ± 0.05	1.29 ± 0.11	0.48 ± 0.04
$E_p - E_\gamma$	low-z	12	50.55 ± 0.09	1.39 ± 0.20	0.26 ± 0.09
	high-z	12	50.30 ± 0.14	1.37 ± 0.44	0.39 ± 0.16
	All-z	24	50.43 ± 0.07	1.39 ± 0.17	0.29 ± 0.07
$\tau_{\text{RT}} - L$	low-z	39	52.52 ± 0.12	-1.24 ± 0.18	0.46 ± 0.06
	high-z	40	52.38 ± 0.08	-0.75 ± 0.17	0.42 ± 0.06
	All-z	79	52.42 ± 0.07	-1.02 ± 0.11	0.43 ± 0.041
$E_p - E_{\text{iso}}$	low-z	40	52.43 ± 0.10	1.49 ± 0.20	0.59 ± 0.08
	high-z	61	52.51 ± 0.06	1.22 ± 0.14	0.39 ± 0.04
	All-z	101	52.47 ± 0.05	1.38 ± 0.12	0.48 ± 0.04

- Our intrinsic scatter for almost all the scaling relations are comparable to that found in T21. The only exception is the Amati relation where we see a much higher intrinsic scatter compared to T21.
- Although there is negligible redshift evolution in the scaling relations, the high intrinsic scatter implies that we cannot use these observables for model-independent estimate of cosmological parameters.

Acknowledgements

This work builds upon the M.Tech thesis of Shreeprasad Bhat and we are grateful to him for sharing his codes.

-
- [1] L. Tang, X. Li, H.-N. Lin, and L. Liu, *Astrophys. J.* **907**, 121 (2021), 2011.14040.
- [2] P. Kumar and B. Zhang, *Phys. Rep.* **561**, 1 (2015), 1410.0679.
- [3] Y.-W. Yu, H. Gao, F.-Y. Wang, and B.-B. Zhang, in *Handbook of X-ray and Gamma-ray Astrophysics. Edited by Cosimo Bambi and Andrea Santangelo* (2022), p. 31.
- [4] A. Singh and S. Desai, *JCAP* **2022**, 010 (2022), 2108.00395.
- [5] S. Desai, arXiv e-prints arXiv:2303.10643 (2023), 2303.10643.
- [6] C. Kouveliotou, C. A. Meegan, G. J. Fishman, N. P. Bhat, M. S. Briggs, T. M. Koshut, W. S. Paciesas, and G. N. Pendleton, *Astrophys. J. Lett.* **413**, L101 (1993).
- [7] S. E. Woosley and J. S. Bloom, *Ann. Rev. Astron. Astrophys.* **44**, 507 (2006), astro-ph/0609142.
- [8] E. Nakar, *Phys. Rep.* **442**, 166 (2007), astro-ph/0701748.
- [9] S. Kulkarni and S. Desai, *Astrophysics & Space Sciences* **362**, 70 (2017), 1612.08235.
- [10] A. Bhave, S. Kulkarni, S. Desai, and P. K. Srijith, *Astrophysics & Space Sciences* **367**, 39 (2022), 1708.05668.
- [11] M. G. Dainotti and L. Amati, *PASP* **130**, 051001 (2018), 1704.00844.
- [12] T. Parsotan and H. Ito, *Universe* **8**, 310 (2022), 2204.09729.
- [13] M. G. Dainotti and R. Del Vecchio, *New Astronomy Reviews* **77**, 23 (2017), 1703.06876.
- [14] O. Luongo and M. Muccino, *Mon. Not. R. Astron. Soc.* **518**, 2247 (2023), 2207.00440.
- [15] M. G. Dainotti, V. Nielson, G. Sarracino, E. Rinaldi, S. Nagataki, S. Capozziello, O. Y. Gnedin, and G. Bargiacchi, *Mon. Not. R. Astron. Soc.* **514**, 1828 (2022), 2203.15538.
- [16] S. Pradyumna and S. Desai, *Journal of High Energy Astrophysics* **35**, 77 (2022), 2204.03363.

- [17] M. Moresco, L. Amati, L. Amendola, S. Birrer, J. P. Blakeslee, M. Cantiello, A. Cimatti, J. Darling, M. Della Valle, M. Fishbach, et al., *Living Reviews in Relativity* **25**, 6 (2022), 2201.07241.
- [18] N. Khadka, O. Luongo, M. Muccino, and B. Ratra, *JCAP* **2021**, 042 (2021), 2105.12692.
- [19] G. Govindaraj and S. Desai, *JCAP* **2022**, 069 (2022), 2208.00895.
- [20] F.-Y. Wang, S. Qi, and Z.-G. Dai, *Mon. Not. R. Astron. Soc.* **415**, 3423 (2011), 1105.0046.
- [21] L. Amati, *Mon. Not. R. Astron. Soc.* **372**, 233 (2006), astro-ph/0601553.
- [22] D. M. Scolnic, D. O. Jones, A. Rest, Y. C. Pan, R. Chornock, R. J. Foley, M. E. Huber, R. Kessler, G. Narayan, A. G. Riess, et al., *Astrophys. J.* **859**, 101 (2018), 1710.00845.
- [23] Y. Dai, X.-G. Zheng, Z.-X. Li, H. Gao, and Z.-H. Zhu, *Astron. & Astrophys.* **651**, L8 (2021), 2111.05544.
- [24] M. Demianski, E. Piedipalumbo, D. Sawant, and L. Amati, *Astron. & Astrophys.* **598**, A112 (2017), 1610.00854.
- [25] M. Demianski, E. Piedipalumbo, D. Sawant, and L. Amati, *Astron. & Astrophys.* **598**, A113 (2017), 1609.09631.
- [26] B. E. Schaefer, *Astrophys. J.* **660**, 16 (2007), astro-ph/0612285.
- [27] R. Sari, T. Piran, and J. P. Halpern, *Astrophys. J. Lett.* **519**, L17 (1999), astro-ph/9903339.
- [28] D. J. Mortlock, S. J. Warren, B. P. Venemans, M. Patel, P. C. Hewett, R. G. McMahon, C. Simpson, T. Theuns, E. A. González-Solares, A. Adamson, et al., *Nature (London)* **474**, 616 (2011), 1106.6088.
- [29] G. Risaliti and E. Lusso, *Nature Astronomy* **3**, 272 (2019), 1811.02590.
- [30] E. Lusso, G. Risaliti, E. Nardini, G. Bargiacchi, M. Benetti, S. Bisogni, S. Capozziello, F. Civano, L. Eggleston, M. Elvis, et al., *Astron. & Astrophys.* **642**, A150 (2020), 2008.08586.
- [31] M. Seikel, C. Clarkson, and M. Smith, *JCAP* **2012**, 036 (2012), 1204.2832.
- [32] H. Singirikonda and S. Desai, *European Physical Journal C* **80**, 694 (2020), 2003.00494.
- [33] K. Bora and S. Desai, *JCAP* **2021**, 052 (2021), 2104.00974.
- [34] K. Bora and S. Desai, *European Physical Journal C* **81**, 296 (2021), 2103.12695.
- [35] K. Bora, R. F. L. Holanda, S. Desai, and S. H. Pereira, *European Physical Journal C* **82**, 17 (2022), 2106.15805.
- [36] R. Agrawal, H. Singirikonda, and S. Desai, *JCAP* **2021**, 029 (2021), 2102.11248.
- [37] I. E. C. R. Mendonça, K. Bora, R. F. L. Holanda, S. Desai, and S. H. Pereira, *JCAP* **2021**, 034 (2021), 2109.14512.
- [38] I. E. C. R. Mendonça, K. Bora, R. F. L. Holanda, and S. Desai, *JCAP* **2021**, 084 (2021), 2107.14169.
- [39] R. F. L. Holanda, K. Bora, and S. Desai, *European Physical Journal C* **82**, 526 (2022), 2105.10988.
- [40] F. Pedregosa, G. Varoquaux, A. Gramfort, V. Michel, B. Thirion, O. Grisel, M. Blondel, P. Prettenhofer, R. Weiss, V. Dubourg, et al., *Journal of Machine Learning Research* **12**, 2825 (2011).
- [41] G. D'Agostini, arXiv e-prints physics/0511182 (2005), physics/0511182.
- [42] D. Foreman-Mackey, D. W. Hogg, D. Lang, and J. Goodman, *Publ. Astron. Soc. Pac.* **125**, 306 (2013), 1202.3665.